MICROSTRUCTURAL CHARACTERIZATION OF SURFACE DAMAGE THROUGH ULTRA-SHORT LASER PULSES

Paper Number M704

Václav Ocelík[1], Jozef Vincenc Oboňa[2], Johann Z.P. Skolski[2], Gert-Willem R.B.E. Römer[3], Albert J. Huis in t' Veld[3] and Jeff Th.M. De Hosson[1]

[1] Department of Applied Physics, Zernike Institute for Advanced Materials, University of Groningen, Nijenborgh 4, 9747 AG Groningen, The Netherlands
[2]Materials innovation institute M2i, Faculty of Engineering Technology, Chair of Applied Laser Technology, University of Twente, P.O. Box 217, 7500 AE, Enschede, The Netherlands
[3]Faculty of Engineering Technology, Chair of Applied Laser Technology, University of Twente, P.O. Box 217, 7500 AE, Enschede, The Netherlands

Abstract

Electron back-scatter diffraction (EBSD) technique, commonly used to study the microstructural characteristics of materials, was employed for the investigation of the surface damage induced through ultra-short laser pulses. Single-crystal silicon surface was irradiated with an Ytterbium-doped YAG (Trumpf-TruMicro 5050) laser source generating laser pulses of 6.7 ps duration, a 1030 nm wavelength and linear polarization. The laser fluence level was set to values lower than the single-pulse modification threshold of the material. The laser pulses were delivered on the surface at conditions of lateral displacement, i.e. a train of laser pulses with a partial overlap (laser track). This approach made it possible to investigate the early stages of modification of the surface. Scanning electron microscope equipped with a field emission gun (Philips XL30 SEM FEG) and EDAX-TSL EBSD system was used for inspection of the surface modifications initiated with pulsed laser radiation. Depth of the generation of back-scattered electrons at different acceleration voltages of the primary beam was estimated by the use of Monte-Carlo simulation. Trajectories of primary and back-scattered electrons in a flat Si surface were generated at an angle of 74º from the surface normal, which is the angle used for the EBSD observations. High sensitivity of EBSD signal allows an estimate of the depth and intensity of the laser induced damage to the crystal lattice. It is found that the thickness of amorphous layer increases gradually with a distance from the feature center. The similarity of surface damage profiles observed at different accelerating voltages of the primary beam indicates that the damage is formed via a gradual crystal damage accumulation in subsurface layer and via the formation and growth of an amorphous layer from the surface.

Introduction

Currently a lot of effort is paid to understand the initiation and "growth" of laser beam induced periodic surface structures (LIPSSs) due to remarkable industrial interest. These modified surfaces are produced in a single-step contact-less process. These periodic modifications have sub-wavelength periodicity and sub-micrometer amplitudes. Colorized and decorated surfaces [1], light trapping [2], control of surface reflection [3], modifications in contact mechanics [4], as well as stimulation and directional growth of living cells [5] are typical examples of considered industrial applications. Laser pulse machining, especially with pulses of picosecond and femtosecond durations, creates a variety of LIPSSs with a strong dependence on the laser light properties (polarization, wavelength), optical properties of the irradiated material and other processing conditions. Two types of the LIPSSs are important for purposes of this paper: low spatial frequency LIPSSs (LSFLs) with periodicity close to that of the initial beam and direction orthogonal to polarization, and high spatial frequency LIPSSs (HSFLs) with periodicity much lower than that of the initial beam and direction parallel to polarization.

Well-developed LIPSSs tend to follow well defined directions orthogonal (LSFLs) or parallel (HSFLs) to polarization when initiated with linearly polarized laser beam. Possibility to obtain a mix of LIPSSs following both directions was presented by modelling on Si at conditions of low excitation of the surface [6]. It was also demonstrated [7] that LIPSSs created at conditions of repetitive irradiation of the surface with low fluence pulses may not strictly follow the polarization direction. Therefore, experiments in the present paper are focused on investigation of initiation of the LIPSSs initiation and early stages of their "growth". The results were produced with an approach based on low-dose repetitive irradiation of the Si

surface. A high resolution in terms of the accumulated fluence was obtained by combination of three processing parameters: i) significantly defocused laser beam in order to get a shallow Gaussian distribution with large $1/e^2$ diameter; ii) multiple exposures; with iii) lateral displacement of the laser pulses.
The subsurface crystal damage during the initiation and subsequent "growth" of LIPSSs, even those not yet reported, were inspected with high resolution scanning electron microscopy combined with electron back-scattered diffraction (EBSD) technique - as a surface sensitive technique to distinguish the quality of the crystal.

Electron back-scattering patterns, also known as Kikuchi patterns, have been applied for many years for measuring of crystal orientations in the scanning electron microscope (SEM). A significant breakthrough for this technique was development of system with a fully automated analysis of the patterns. It enables the collection of huge amounts of crystal orientation data [8]. Maps generated from automated electron backscatter diffraction (EBSD) also called orientation imaging microscopy OIM [9] are powerful instruments to visualize polycrystalline microstructures. One of the common maps constructed from EBSD data is the Image Quality (IQ) map that describes the value measured for each diffraction pattern obtained during OIM scan. Definition of conventional IQ parameter is based on Hough Transform [10] as an image processing procedure for locating the bands in EBSD pattern by their transformation into intensity peaks. The IQ parameter describes the average height of these peaks.

There are few factors that influence value of IQ parameter substantially:

- maximum number of detected peaks is a user-defined value and thus IQ depends this way on the user's selection;
- the "perfection" of crystal lattice and the atoms present within the diffraction volume both affect diffraction pattern quality. In the case of plastic deformation or radiation damage the diffraction volume would no longer contain a single crystal lattice but a set of lattices of slightly different orientations with respect to one another. The resulting pattern is then a superposition of the individual patterns from the individual lattices, leading to a more diffuse Kikuchi pattern with lower IQ parameter [11];
- chemical elements present within the diffracting volume will also affect the IQ. Heavier materials tend to have higher atomic scattering factors for electron diffraction, resulting in brighter patterns.

Generally, contrast observed in maps constructed using the IQ parameter can arise from strain, grain boundaries, phase, surface topology and/or other features of the microstructure [11]. The absolute values of the various IQ parameters are also affected by the gain and contrast settings of the EBSD detector unit, as well as the scanning electron microscope. Thus, absolute values of IQ parameter are not particularly useful. However, the relative value between points in one OIM scan is useful and the contrast observed in maps generated from the IQ values can be correlated to features of the microstructure [11].

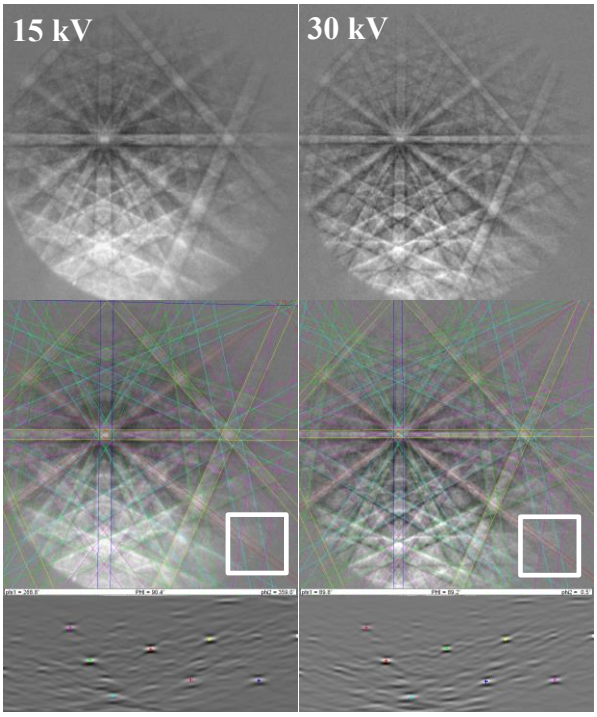

Fig. 1: Kikuchi patterns obtained from Si crystal surface taken at 15 kV (left column) and 30 kV (right column). Appropriate indexing determines the crystal orientation shown as inserts in indexed patterns: (100) plane is perpendicular to sample surface normal *z* and [100] direction is parallel to the reference (vertical) direction. The lowest part of the figure shows corresponding Hough transformation patterns with 8 detected bands.

Figure 1 shows typical Kikuchi patterns observed on silicon using two different primary electron beam energies. Indexing of the patterns determines the crystal orientation in the sample coordinate system. The average intensity of 8 detected peaks in Hough space determines the value of IQ.

EBSD is performed at high tilts (typically ~70º) in scanning electron microscope and the interaction volumes are relatively small. Therefore it is a very

surface sensitive technique. EBSD based IQ maps were for the first time correlated to the grade of the silicon crystallinity after irradiation by laser beam in experimental work of Gimpel et al. [12]. Presence of an amorphous layer at the top surface of irradiated silicon wafer was supposed to decrease IQ parameter in OIM maps. In another recent experimental work EBSD has been used to determine the dependence of LIPSSs formation upon the crystal orientation in a poly-crystalline nickel [13].

The goal of our investigation was to prove experimentally how the diffraction of back-scattered electrons could be used to detect and characterize a size and depth of subsurface damage created during low-dose ultra-short irradiation by pulsed laser.

Experimental

An Ytterbium-doped YAG (Trumpf TruMicro 5050) laser source, producing laser pulses of 6.7 ps duration and a wavelength of 1030 nm, was used. The linearly polarized laser beam was delivered to the silicon wafer surface by an f-theta lens (255 mm focal distance, Jenoptik, Germany) at normal incidence angle. Prior the experiments the laser beam was defocused in order to get a $1/e^2$ diameter as broad as possible, e.g. 155.76 µm. A Gaussian energy distribution was confirmed in focus, as well as for the defocused beam.

Low fluence accumulation (LFA) experiments were performed with peak fluences ranging from 0.20 to 0.26 J/cm^2, laser pulse overlaps (OL) from 71 to 99.9 % and number of over-scans (OS) from 10 to 100. High fluence accumulation experiments (HFA) were done at two fluences equal to 0.43 and 0.45 J/cm^2, OL was fixed at 50% and 10 OS were applied. All experiments were done at 1 kHz laser pulse frequency. Scanning directions were parallel or orthogonal to polarization vector, which deviated 10° anticlockwise from the horizontal direction. More experimental details concerning laser processing will be found in [14].

A Philips XL30 scanning electron microscope, equipped with field emission gun (SEM-FEG) and TSL EBSD detector was used to reach a resolution of few nanometers in order to perform a detailed inspection of the topography of the samples on secondary electron (SE) images. EBSD detector was used for crystallographic analyses and OIM scans. Image quality maps were combined with Inverse Pole Figure (IPF) maps [15]. Imaging in SE was performed at low acceleration voltage (8 kV) and small working distance of 5 mm to achieve maximal lateral resolution.

EBSD experiments were performed using various acceleration voltages of primary beam (10-30 kV), fixed beam current and working distance (15 mm). Imaging conditions for CCD camera collecting Kikuchi patterns from a phosphorus detector were also fixed to keep the same resolution and speed of pattern collection. Also the number of detected bands in Hough space was kept constant, namely 8. OIM scanning steps were selected between 50-150 nm with a hexagonal grid.

The penetration depth of diffracted back-scattered electrons for different energies of primary electron beam was estimated by Monte-Carlo simulation [16] of electrons trajectories in Si with the surface normal inclined 74º to electron beam (corresponding to the experimental set-up).

Results and Discussion

First signs of the initiation of LIPSSs formation on Si surface in the LFA experiments can be seen in Fig. 2. The initiation sites were difficult to find due to poor contrast, their very small dimensions in comparison to the spot diameter, and due to the stochastic nature of their presence inside the irradiated laser track. Figure 2b suggests that the basic shape of the modifications is represented with a central line accompanied with two side-lobs. The orthogonal alignment of the features to the polarization direction is apparent. The lateral dimensions of these initiation sites were in the sub-micron range. Darker places on the SE micrographs were under the initial surface level, as suggested by the lower production of secondary electrons and hereafter proven by the observations on inclined surfaces. Few of these lines and side-lobs tend to be broader in the center of the structures. The initiation was similar for various combinations of OL and OS at the same peak fluence level. Particles covering the surface in Fig.2 were produced by the re-deposition of material, ablated in the vicinity of these side-blobs features.

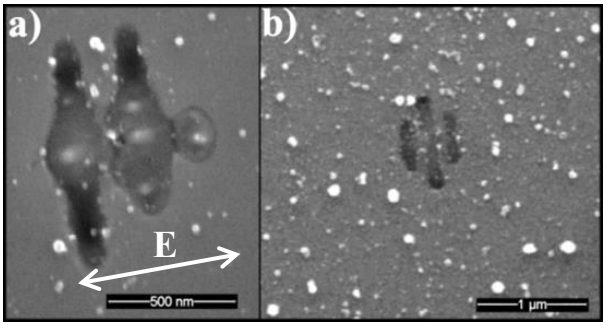

Fig. 2: First stages of LIPSSs initiation in LFA experiment observed in SE. Polarization direction is marked by double-headed arrow.

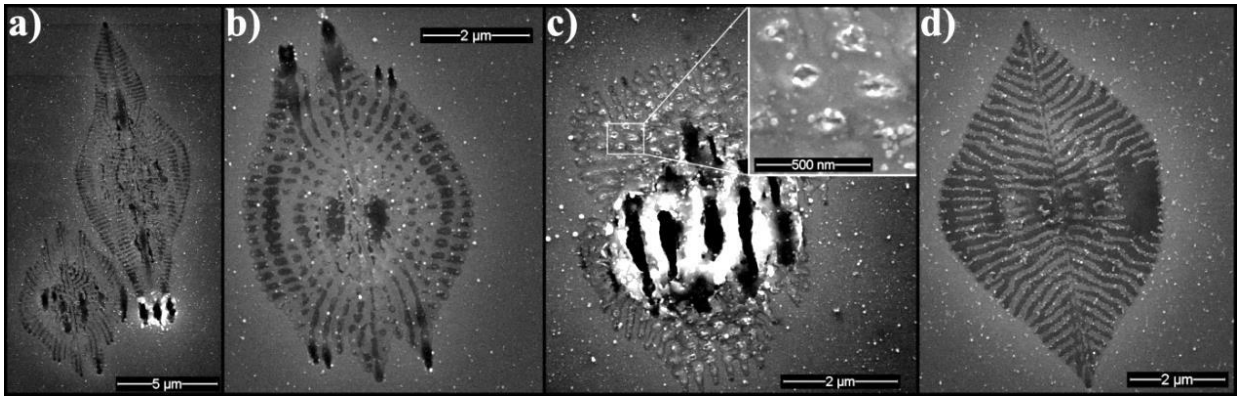

Fig. 3: Complex surface structures observed in SE. Irradiation conditions were as follows: a) 0.26 J/cm^{-2} fluence, 87% OL, 40 OS; b) 0.26 J/cm^{-2} fluence, 97% OL, 10 OS; c) J/cm^{-2} fluence, 95% OL, 100 OS; d) 0.26 J/cm^{-2} fluence, 79% OL, 60 OS.

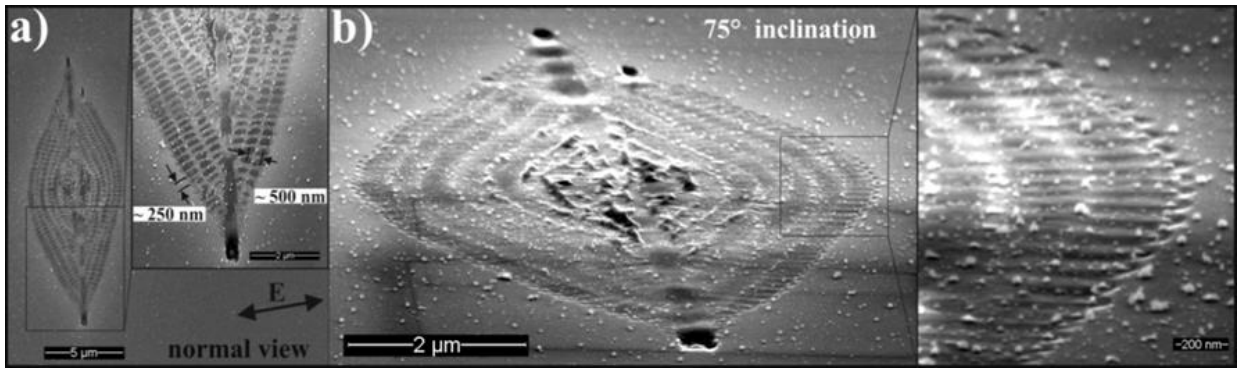

Fig. 4: Leaf-like pattern showing the superposition of various periodicities of LIPSSs. The irradiation conditions for this laser track were: 0.26 J/cm^{-2} fluence, 97% OL, 10 OS. a) SEM-FEG normal view with indication of two periodicities and direction of polarization vector. b) SEM-FEG micrograph of the same pattern inclined 75° outward (upper side of the sample further from the pole-piece) showed detailed topography of the structure.

More developed surface modifications in LFA experiment are shown in Fig. 3. Complex periodicities appeared in the form of leaf-like patterns. At least five concentric dashed-line ovals can be identified in pattern in Fig 3b. A certain level of symmetry was typical for these patterns. Long symmetry axis of the feature is orthogonal to the polarization direction. At high OL, further increase of OS induced the creation of structures similar to bursting cupolas (Fig 3c inset). A decrease in variety of the periodicities appeared with a decrease of OL (Fig 3d).

Figure 4 summarizes a detailed inspection of one complex and nicely-developed leaf-like pattern. The pattern is composed of a central line, orthogonal to the polarization direction, with concentric dashed-line ovals attached to it. The distance between the dashed-line concentric ovals was about 500 nm and it was approximately twice the periodicity along the dashed lines (Fig. 4a). The inclination of the surface at an angle of 75° towards electron beam improves the visibility of the surface topography. A material removal or movement is visible mainly along the central line but it is recognizable in the whole modified area.

A few complex patterns were chosen for the investigation of the crystalline state of the surface with the EBSD/OIM technique.

Figure 5 shows an SE image with two OIM maps collected from the feature previously shown in details in Fig.4. Resolution of SEM image is in this case much worse due to the higher acceleration voltage (10-30 kV) and stronger primary beam, required to observe EBSD patterns. OIM map in the middle of this figure combines Inverse Pole Figure map (IPF) in color with the IQ map represented by brightness. Attached color legend indicates the crystallographic orientation of the silicon wafer in a vicinity of the feature. This orientation is also depicted in the upper right corners of OIM maps as a small axonometric projection of cubic crystal. The sharp loss of brightness in IQ map is

attributed to the presence of a thin surface amorphous layer inside the feature. Image quality parameter falls to the zero value inside this area, which means that no bands were detected on corresponding images collected during EBSD scanning. Thickness of the amorphous layer exceeds the penetration depth of diffracted back-scattered electrons, which will be discussed later.

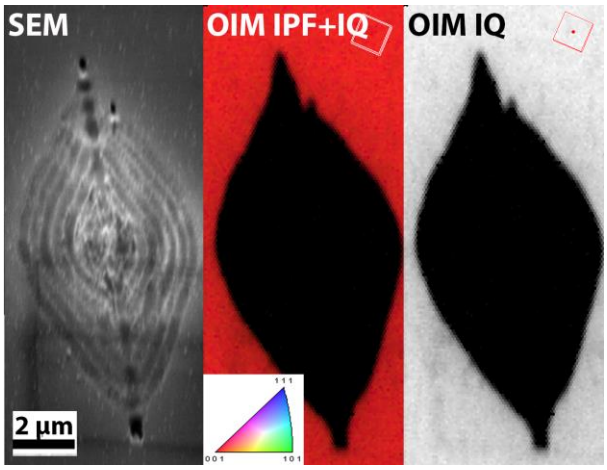

Fig. 5: SE image and OIM maps of the feature shown in Fig.4.

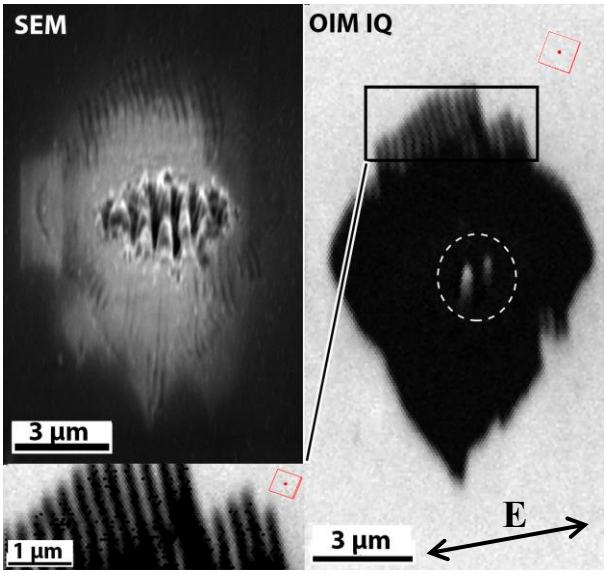

Fig. 6: SE image and OIM IQ map of the LFA feature.

Another typical feature observed in LFA experiments is shown in Fig. 6. Here a combination of SEM image with IQ maps is depicted. The conditions of laser processing were: 0.20 J/cm^{-2} fluence, 88.34% OL and 100 OS. The initiation of LSFLs happens in this pattern from its center. Another observed preferential initiation sites were the ends of the midrib of the leaf-like patterns (see Fig. 3a, b). The periodicity of these LSFLs varied in the range from 655 to 964 nm, which equals to a range of 0.64 λ to 0.94 λ, the direction was always orthogonal to the polarization vector. The development of LSFLs seemed to only happening in the modified area of the patterns. That is, LSFLs fill preferentially the area defined by the leaf like pattern and they do not "grow" outside these areas. The surroundings of these patterns were found to be covered by small particles due to re-deposition of ablated material. IQ map shown in Fig. 6 manifests a slightly different surface modification than inside the feature observed in Fig. 5. Upper and bottom border of the area with decreased IQ signal does not show a sharp change. System of "fingers" with a decreased IQ signal propagates from the feature in both directions perpendicular to the polarization direction (see OIM map of magnified area). Periodic changes of IQ signal in polarization direction was measured to be very close to λ/4. The area around the central part of the feature seems to be fully amorphous. However, on the tops of the initiated LSFLs, at the center of the feature, crystalline areas were detected (see area marked by dashed circle) with the same orientation as was the crystal orientation of the Si wafer. The orientation is depicted in the same way as in Fig. 5.

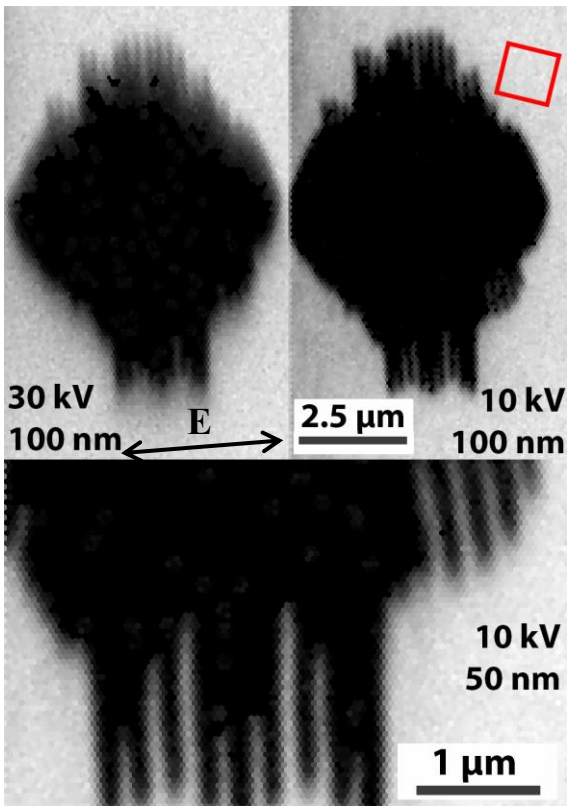

Fig. 7: OIM IQ maps collected from one feature at different primary beam energy and distance between scanning points.

The role of experimental conditions during the collection of OIM maps by EBSD is clearly demonstrated in Figure 7, where IQ maps collected from the same feature at different experimental conditions are shown. Two upper maps show clearly an influence of acceleration voltage. This influence is possible to observe in the upper part of the feature. While in the at 10 kV map the fingers became fully dark (IQ = 0) at their ends, at 30 kV map these places show only a decrease in IQ parameter. This means that at lower voltage the back-scattered electrons did not create diffraction pattern in these points. However, back-scattered electrons originated from beam with higher energy are still diffracted, although with less intensity than on non-touched surface. The detailed scan at the bottom of Fig. 7 shows a scan with the highest resolution. A detail of the bottom part of the feature is scanned here with a 50 nm distance between individual points. Resolution of EBSD technique has analytical and spatial resolution limits consistent with electron scattering phenomena in bulk materials [17].

The depth resolution is highly material dependent, but it also depends on acceleration voltage of incident beam. To obtain a physical picture, what is depth resolution in EBSD and how it depends on acceleration voltage, we performed few Monte-Carlo simulations of electron scattering trajectories in EBSD configuration using approach developed in [16].

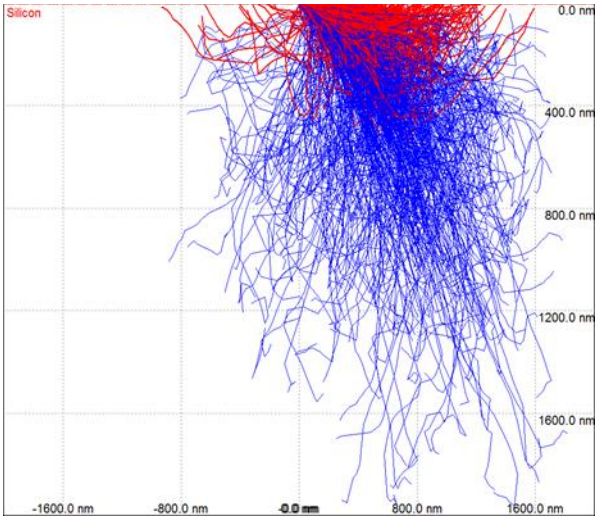

Fig. 8: Results of Monte-Carlo simulation of trajectories of 20 kV electrons in silicon. Primary electron beam is titled 74º toward the Si surface normal. Trajectories of back-scattered electrons are highlighted in red. Only first 10^3 trajectories from overall 10^5 are shown due to readability.

Figure 8 shows result of one simulation of penetration trajectories of electrons in Si crystal. This simulation is for 20 kV primary electron beam with a diameter of 5 nm typical for FEG SEM. This beam hits the surface whose normal is tilted 74º towards primary electron beam at coordinates (0, 0). Trajectories of back-scattered electrons inside silicon sample are shown in Fig.8 as red trajectories. It is clear that the penetration depth of back-scattered electrons is much smaller than the penetration depth of all injected electrons. However, only back-scattered electrons which are leaving the sample surface with energy close to the energy of primary beam would contribute to the diffraction pattern (15-20%) [15]. These electrons are therefore back-scattered from depths very close to the surface and loose only a small part from their original energy. The penetration depth of diffracted back-scattered electrons is therefore estimated here as a depth of the first 20% from penetration depth distribution of all back-scattered electrons (blue area in Fig. 9 for 30 kV distribution). Figure 9 also summarizes our Monte-Carlo simulations for other acceleration voltages to show how the penetration depth depends on acceleration voltage. This dependence seems to be linear in the range of 10-30 kV and varies between 6 and 35 nm (see inset in Fig. 9).

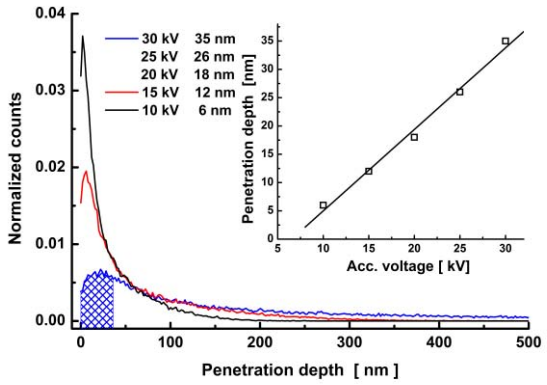

Fig. 9: Distribution of penetration depths of back scattered electrons on Si surface with normal tilted 74º towards primary electron beam with different initial energy (only distributions for 30, 15 and 10 kV are shown due to redability). Integral under 30 kV line shows penetration depth for diffracted electrons. Insert shows a dependence of penetration depth of diffracted electrons on acceleration voltage of primary beam.

Considering the analysis above and differences observed in Fig. 7 for 30 and 10 kV EBSD maps we may conclude that the thickness of amorphous layer at the ends of fingers is larger than 6 and smaller than 30 nm. Thickness of the crystal damage in the central part of features shown in Fig. 5 and Fig. 7 is larger than 35 nm.

The lateral spatial resolution of EBSD can be viewed as the size of the area out of which electrons are back-scattered. Factors such as atomic number and density of the specimen, size and energy of the primary electron beam play important roles in determining this resolution [17]. The best values reported in literature are approximately 80 to 90 nm in direction perpendicular (vertical in our images) and 20 to 35 nm in direction parallel (horizontal in our images) to the tilt axis [17]. In our experiment the lateral resolution of EBSD on Si at 10 kV seems to be better than 100 nm. We observe an improvement of details between fingers in Fig. 7 for distance between scanning points of 50 nm in comparison to 100 nm. Period of IQ signal modulation in direction of polarization vector has been estimated. IQ signal on detailed scan from Fig. 7 was analyses and period of 270 nm was found , which is again very close to $\lambda/4$.

The initiation of LIPSSs in the HFA regime was conducted at peak fluence levels approximately twice higher than in LFA experiments. The percentage of OL and the number of OS had to be lowered accordingly, in order to get only a partial modification of the surface within the laser track. The smallest observed surface modifications consisted of three attached ovals with sub-micron lateral dimensions [14]. Further irradiation led to more significant signs of surface melting than in LFA experiment. A typical example of a developed feature in HFA regime (fluence 0.43 J/cm^2, 50 OL, 10 OS) is shown in Fig. 10. SEM image clearly confirms that a reinforced absorption in the center of the feature destroys originally formed periodic pattern due to intensive contribution of melting and material transport. The darker arcs, further from the center of the modification had almost a negligible topography, as can be observed on the inclined surfaces in magnified insert of the SEM micrograph. Closer to the center of the feature a significant surface melting happened, visible as elevated rims. Closer inspection by EBSD clearly discloses that the central part of the feature (with the clear signs of melting on SEM image) is crystalline with the same crystal orientation as is the orientation of wafer substrate. This means that solidification after melting was controlled by epitaxial growth from the bottom. Surrounding part shows a clear amorphous layer, with a thickness higher than 6 nm (10 kV primary beam was used). Further away from the center a periodic modulation of IQ signal occurs in falciform dark areas with decreasing minimum amplitude as a function of distance from the center. Period of these modulations was measured in direction of polarization as 950 nm, which is close to the wavelength of the laser radiation used in experiment. A discrepancy is probably due to the orientation of the tilting axis in our experiment (horizontal in Fig. 10), that induces a larger error in measuring vertical distances on the figure. The vertical impressions of horizontal LIPSSs in the IQ map in Fig. 10 could be explained by a shielding of primary, as well as back-scattered electrons by non-uniformly elevated rims present in melted central part of the feature (SEM image in Fig. 10).

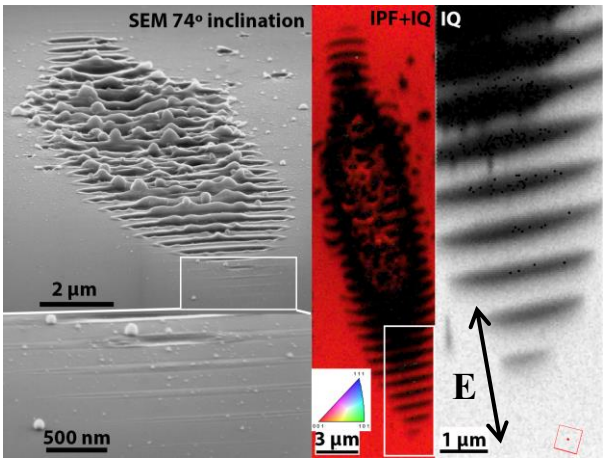

Fig. 10: SEM and OIM observation of the feature formed in HFA experiment. 74º degree tilted SE image is presented on the left side with the magnified bottom periphery under it. Inverse pole figure map of the whole feature combined with IQ information is in the central-color part of the figure (10 kV, 150 nm). On the right side the IQ map of the bottom periphery of the feature is presented (10 kV, 50 nm).

It was not the aim of this contribution to explain mechanisms of the LIPSSs formation on Si substrate in these LFA and HFA experiments. A more detailed physical picture that uses EBSD observations is presented in [14]. The objective of this paper is to demonstrate how advantages of EBSD technique inside a scanning electron microscope could be applied in a detailed study of surface and subsurface damage formed during irradiation with picosecond laser pulses.

Conclusions

Orientation imaging microscopy is a versatile instrument for the characterization of crystal surface damage formed on the laser beam irradiated surfaces. The onset of damage, when the amorphous layer is only ~ 10 nm thick could be detected using Image Quality mapping. Moreover, an exact crystal orientation towards scanning of the laser beam and its polarization direction could be precisely determined using the possibility to determine precisely the crystal orientation in the sample coordinate system inside scanning electron microscope.

Some features formed by picosecond laser pulses are visible in images using secondary electrons but subsurface damage and loss of crystalline order is clearly visualized in EBSD OIM map that uses the Image Quality parameter.

Acknowledgement

This research was partially carried out under project number M61.3.08300 in the framework of the Research Program of the Materials innovation institute M2i (www.m2i.nl).

References

[1] Dusser, B., Sagan, Z., Soder, H., Faure, N., Colombier, J.P., Jourlin, M. & Audouard, E. (2010) Controlled nanostructrures formation by ultra fast laser pulses for color marking, Optics Express 18, 2913–24.

[2] Scorticati, D., Römer, G.R.B.E., De Lange, D.F. & Huis In 't Veld, B. (2012) Ultra-short-pulsed laser-machined nanogratings of laser-induced periodic surface structures on thin molybdenum layers, Journal of Nanophotonics 6, 063528–063528.

[3] Vorobyev, A.Y., Makin, V.S. & Guo, C. (2009) Brighter light sources from black metal: Significant increase in emission efficiency of incandescent light sources, Physical Review Letters 102, 234301.

[4] Tagawa, N., Takada, M., Mori, A., Sawada, H. & Kawahara, K. (2006) Development of contact sliders with nanotextures by femtosecond laser processing, Tribology Letters 24, 143–9.

[5] Rebollar, E., Frischauf, I., Olbrich, M., Peterbauer, T., Hering, S., Preiner, J., Hinterdorfer, P., Romanin, C. & Heitz, J. (2008) Proliferation of aligned mammalian cells on laser-nanostructured polystyrene, Biomaterials 29, 1796–806.

[6] Skolski, J.Z.P., Römer, G.R.B.E., Vincenc Obona, J. & Huis In 'T Veld, A.J. (2014) Modeling laser-induced periodic surface structures: Finite-difference time-domain feedback simulations, Journal of Applied Physics 115, 103102.

[7] Crawford, T.H.R. & Haugen, H.K. (2007) Sub-wavelength surface structures on silicon irradiated by femtosecond laser pulses at 1300 and 2100 nm wavelengths, Applied Surface Science 253, 4970–7.

[8] Wright, S. & Adams, B. (1992) Automatic-Analysis of Electron Backscatter Diffraction Patterns, Metallurgical Transactions a-Physical Metallurgy and Materials Science 23, 759–67.

[9] Adams, B.L., Wright, S.I. & Kunze, K. (1993) Orientation imaging: The emergence of a new microscopy, Metallurgical Transactions A 24, 819–31.

[10] Krieger Lassen (1998) Automatic high-precision measurements of the location and width of Kikuchi bands in electron backscatter diffraction patterns, Journal of Microscopy 190, 375–91.

[11] Wright, S.I. & Nowell, M.M. (2005) EBSD Image Quality Mapping, Microscopy and Microanalysis 12, 72–84.

[12] Gimpel, T., Höger, I., Falk, F., Schade, W. & Kontermann, S. (2012) Electron backscatter diffraction on femtosecond laser sulfur hyperdoped silicon, Applied Physics Letters 101, 111911.

[13] Sedao, X., Maurice, C., Garrelie, F., Colombier, J.-P., Reynaud, S., Quey, R. & Pigeon, F. (2014) Influence of crystal orientation on the formation of femtosecond laser-induced periodic surface structures and lattice defects accumulation, Applied Physics Letters 104, 171605.

[14] Obona, J.V., Skolski, J.Z.P., Eichstädt, J., Ocelík, V., Römer, G.R.B.E., De Hosson, J.T.M. & Huis In 'T Veld, A.J. (2014) Modification of Si surface with defocused picosecond laser pulses, submitted.

[15] Schwartz, A.J., Kumar, M., Adams, B.L. & Field, D.P. (2009) Electron Backscatter Diffraction in Materials Science (Boston, MA: Springer US)

[16] Drouin, D., Couture, A.R., Joly, D., Tastet, X., Aimez, V. & Gauvin, R. (2007) CASINO V2.42 - A fast and easy-to-use modeling tool for scanning electron microscopy and microanalysis users, Scanning 29, 92–101.

[17] Keller, R.R. & Geiss, R.H. (2012) Transmission EBSD from 10 nm domains in a scanning electron microscope: Transmission EBSD in the SEM, Journal of Microscopy 245, 245–51.

Meet the authors

Václav Ocelík is a research staff working at the Applied Physics Department, Faculty of Mathematics and Natural Sciences of the University of Groningen, The Netherlands. He obtained his MSc in Materials Science at the Faculty of Nuclear Sciences and Physical Engineering, Czech Technical University in Prague and his PhD in Solid State Physics at Šafárik University in Košice, Slovakia. His scientific interests are electron microscopy, microstructure and properties of rapidly solidified materials.

Jeff Th.M. De Hosson is a Professor of Applied Physics at the Faculty of Mathematics and Natural Sciences of the University of Groningen, The Netherlands. He obtained his MSc in Theoretical Physics from the Utrecht University and his PhD in Physics from the University of Groningen, The Netherlands. His research interests are in dislocation dynamics, interface science and in situ transmission and scanning electron microscopy. He is an Elected Member of the Royal Netherlands Academy of Sciences, Royal Holland Society of Sciences and Humanities, Fellow of several international scientific societies and recipient of the European Materials Gold Medal (2005) and TMS–Triple M Society USA Fellow Award (2009).